NUMERICAL SIMULATION OF HIGH PRESSURE SECONDARY ATOMIZATION. EFFECTS OF INITIAL DROPLET SIZE ON FINAL SPRAY STRUCTURE

Emmanuel BODÈLE[†], Iskender GÖKALP[†], Stephan ZURBACH[‡], Didier SAUCEREAU[‡]

[†]Centre National de la Recherche Scientifique
Laboratoire de Combustion et Systèmes Réactifs
1c, avenue de la Recherche Scientifique
45 071 Orléans cedex 2, France

[‡]SNECMA Moteurs
Groupe SNECMA
BP 802-Forêt de Vernon
27 208 Vernon, France

ABSTRACT

This paper presents the elaboration of a secondary atomization model issued from an experimental study previously conducted at LCSR. This experimental work has permitted to characterize the breakup process of a liquid oxygen droplet under high pressure (up to 12 MPa) conditions in terms of breakup initiation time, secondary droplet distribution and breakup mode. The model has been used to compute the ONERA's MASCOTTE configuration in non reactive cases. Conserving initial liquid and gas mass flow rates, the initial droplet size distributions have been varied to characterize the influence of liquid injection conditions on the final spray structure, especially total droplet number, arithmetic and Sauter mean diameters. Finally, we discuss influence of initial droplet distribution on final flow properties (H_2 and O_2 mass fractions).

INTRODUCTION

The efficiency of a cryogenic rocket engine is widely influenced by the elementary processes conducting to spray formation and combustion. Among these elementary phenomena, one of the most influencing parameter is certainly the atomization (primary and secondary atomization) of the liquid introduced in the combustion chamber. The complexity of this phenomenon is one of the reasons why it is not yet well understood. In the case of a rocket engine, the atomization process gains in complexity because of the interaction between injectors (in the Vulcain engine of the European launcher Ariane V, there is more than 500 injectors), the cryogenic temperature for the liquid injected (about 80 K for liquid oxygen), the high pressure in the combustion chamber (more than 10 MPa in certain cases) conducting to supercritical conditions for the liquid, and the high injection velocity for the gas (more than 300 m/s for the Vulcain engine injectors). Because of supercritical effects (dense gas behavior, vanishing superficial tension, ...) the classical approaches for the liquid phase become unsatisfactory. It is necessary to have a detailed comprehension of this physical process in such engines. Modeling and simulation of elementary phenomena are one of the ways to characterize more precisely the cryogenic rocket engine combustion.

The liquid spray formation is generally decomposed in two more elementary processes. The first step called primary atomization consists in the formation of "large" fragments by the action of shear forces generated by the high relative velocity at the droplet surface. The second step consists in reduction of liquid fragment sizes by successive breakups. This second step is controlled by the Weber (We) and Reynolds (Re) numbers (Eq. 1):

$$We = \frac{\rho_g \left(U_g - U_l\right)^2 D}{\sigma}, \; Re = \frac{\rho_g \left|U_g - U_l\right| D}{\mu_g} \tag{1}$$

The Weber number is often considered as the main parameter for the secondary atomization process. A critical Weber number We_c is then defined and its generally admitted value is $We_c = 12$ [1,2]. For values lower than We_c, no fragmentation process can be observed. For larger values, several breakup regimes can be observed. The designation of these breakup modes varies. One of the most complete classification is the Shraiber *and al.*'s classification [3], in which 8 regimes are described. The transition between these regimes is based on the $We/\sqrt{Re}$ criterion previously introduced by Taylor [4] and Gelfand [5]. The number and size of secondary fragments generated during the breakup process is dependent on the fragmentation mode. The dynamic of the fragmentation is controlled by several characteristic times such as initiation time T_{ini} [1] or total breakup time T_{BU} [1]. The initiation time is defined as the duration between the first droplet deformation and the generation of first secondary fragments. In fact this time is equal to the time of deformation of the initial droplet.

SECONDARY ATOMIZATION MODEL

The secondary atomization model [6] is based on an experimental study previously conducted at LCSR [7,8], which has permitted to characterize the droplet breakup in terms of initiation time T_{ini}, secondary droplet distributions and droplet breakup mode. During this experimental work, according to Shraiber *and al.* classification [3], three breakup regimes were observed. For the transition between these regimes, Vieille [7] has established correlations (Eq. 2) based on criterion previously introduced by Taylor [4] and Gelfand [5] which permit, knowing gas and liquid properties, to determine the breakup mode.

$$\frac{We}{\sqrt{Re}} = C \left(\frac{\rho_l}{\rho_g}\right)^{0.25} \left(\frac{\mu_l}{\mu_g}\right)^{-0.5} \tag{2}$$

The breakup regime is then determined by the evaluation of the C value. For each transition, values for the criterion C are reproduced in table 1. If the breakup criterion C is sufficient to generate a breakup, an initiation time T_{ini} is evaluated by equation (3) [7].

$$T_{ini} = 0.75\, T\, We^{-0.06}, \text{ with } T = \frac{D}{U}\sqrt{\frac{\rho_l}{\rho_g}} \tag{3}$$

Breakup regime	C
No breakup	< 0.25
Bag	$0.25 - 0.7$
Transitional	$0.7 - 0.9$
Shear	> 0.9

Table 1: Breakup criterion.

It is remarkable that this initiation time is only slightly dependant on the Weber number, and doesn't depend on the breakup mode. The characteristic time T [9] (Eq. 3) is often used to normalize the initiation time T_{ini} and is obtained considering momentum conservation at liquid/gaz interface.

The last parameter to take into account for the breakup model is the secondary droplet distribution. For each breakup mode and each experimental condition, Vieille [7] has determined number and size of secondary droplets at the breakup time T_{ini}. With these results, we have built simplified secondary droplet distributions depending on primary droplet diameter. These distributions are reproduced in table 2.

	Percentage of initial droplet diameter			**Residual of**
Breakup regime	10 %	30 %	50 %	**initial droplet**
Bag breakup	2	2	1	93.56 %
Transitional breakup	3	1	1	94.54 %
Shear breakup	4	2	1	93.48 %

Table 2: Simplified secondary droplet distributions.

To assume liquid mass conservation, the diameter of initial droplet is adjusted (called residual of initial droplet in table 2). Finally, the fragmentation of a droplet can be considered as a generation of small secondary fragments from initial droplet with conservation of a large residual. All these parameters constituting the secondary atomization model (breakup criterion, secondary distributions, breakup initiation time) have been introduced in the SNECMA's THESEE CFD code and used to compute the ONERA's MASCOTTE [10] test bench.

NUMERICAL CONFIGURATION AND INITIAL DISTRIBUTIONS

The numerical configuration is the same as the one used during the "2nd International Workshop on Liquid Rocket Combustion Modeling" in Lampoldshausen 2001 [11]. Liquid and gas injection conditions are summarized in table 3. Dimensions

	Hydrogen (GH_2)	Oxygen (LOX)
Pressure (MPa)	1.0	1.0
Mass flow rate (g/s)	23.7	50.0
Temperature (K)	287	85
Density (kg/m^3)	0.84	1 170
Heat capacity (J/kg/K)	14 300	1 690
Velocity (m/s)	319	2.18
Viscosity (kg/m/s)	8.6×10^{-6}	1.94×10^{-4}
Surface tension (N/m)	–	1.44×10^{-2}

Table 3: Liquid and gas injection conditions.

of computational domain are the same as the ONERA's MASCOTTE test bench, used to reproduce the conditions encountered in a real rocket engine. This experimental setup is composed of a single coaxial injector using liquid oxygen (LOX) in the inner part, surrounded by high velocity gaseous hydrogen (GH_2) (figure 1). The computational domain obtained with this configuration is reproduced on figure 2 and is 40 cm long and 2.7 cm height. It is composed of 8 838 nodes and 4 223 hexahedral elements.

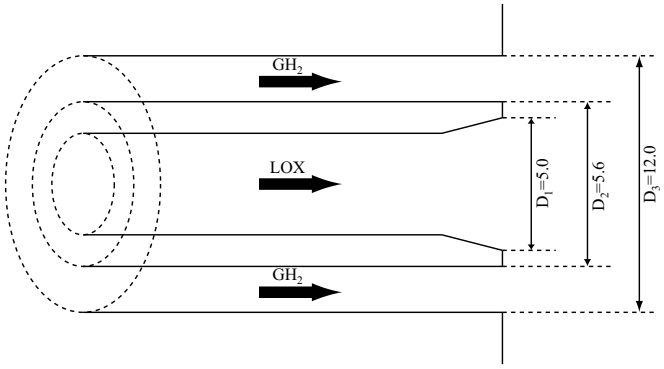

Figure 1: Geometry of the injector (values in mm).

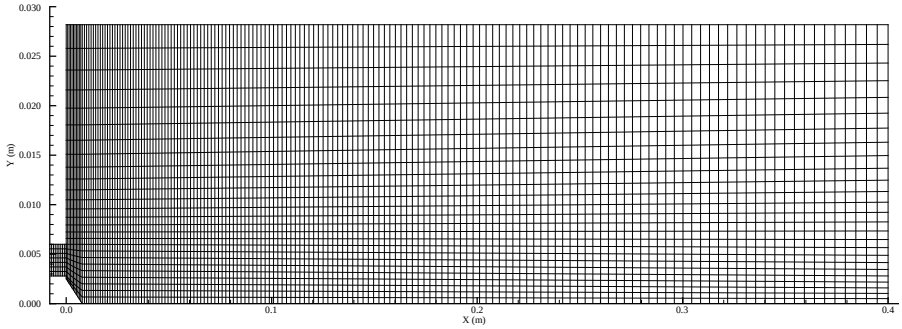

Figure 2: Computational domain.

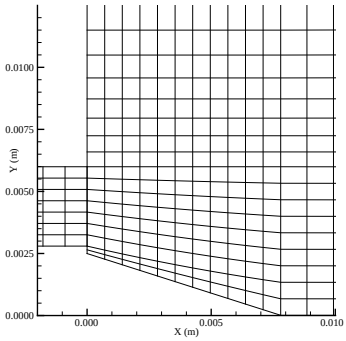

Figure 3: Computational domain (detail).

Liquid oxygen droplets are introduced in the computational domain on the surface of a liquid core (represented on the detailed injection zone on figure 3). The length of this liquid core L_C is given by the Villermaux's relation [12] (Eq. 4), and is equal to 7.8 mm.

$$L_C = \frac{6D_1}{\sqrt{J}}, \text{ with } J = \frac{\left(\rho U^2\right)_{GH_2}}{\left(\rho U^2\right)_{LOX}} = 14.5 \text{ and } D_1 = 5.0 \text{ mm} \tag{4}$$

Simulations are conducted conserving liquid and gas mass flow rates. We only change the initial droplet size distribution to point out the influence of initial droplet size on final spray structure and on final flow properties. The first initial distribution is a Rosin-Rammler distribution which has been previously observed by Care [13] (Eq. 5):

$$1 - \nu_c\left(D\right) = \exp\left[-\left(\frac{D}{D_{RR}}\right)^N\right], \text{ with } D_{RR} = 130\,\mu\text{m and } N = 2.25 \tag{5}$$

The Sauter mean diameter D_{32RR} of this Rosin-Rammler distribution is equal to 82 µm. Four monodisperse distributions are also considered (we have then $D_{32} = D_{10} = D_{ini}$). The first one permits to reproduce the Sauter mean diameter of the previous Rosin-Rammler distribution, and the initial diameter is then $D_{ini} = D_{32RR}$ =82 µm. Initial diameters for other distributions are 50 µm, 100 µm and 150 µm. Finally, a simulation with the Rosin-Rammler distribution (Eq. 5) and without secondary atomization has also been considered to point out the influence of breakup process on final spray properties. Initial droplet injection angle θ and velocity U_0 depend on injection location x on the surface of the liquid core by the following relations [13] (Eqs. 6 for θ and 7 for U_0).

$$\theta\left(x\right) = \arctan\left[\frac{\frac{D_1}{2}\left(1 - \frac{x}{L_C}\right)}{x + \frac{D_1}{2\tan\theta_1}}\right], \text{ with } \tan\theta_1 = 0.68\left(\frac{U_g}{U_l} - 1\right)\sqrt{\frac{\rho_g}{\rho_l}} \tag{6}$$

$$U_0\left(\theta\right) = \frac{0.66}{\cos\left(\frac{\pi}{2} - \alpha - \theta\right)}, \text{ with } \alpha = 17.7\,^\circ \tag{7}$$

All simulations are conducted using a classic D^2 law to reproduce liquid vaporization process. Computations are realized over 200 000 iterations with a time step equal to 8.8×10^{-8} s. The total physical duration is then about 17.6 ms. Results presented in the following sections correspond to average values realized on the last 100 000 time steps.

RESULTS AND DISCUSSION

Spray properties

Table 4 presents total droplet number in the computational domain for all simulations carried out. First, these values point out the influence of the atomization process on final droplet number. All computations considering secondary atomization

Initial distribution	Droplet number
Rosin-Rammler (without atomization)	3 181
Rosin-Rammler (with atomization)	37 419
Monodisperse 50 µm	33 351
Monodisperse 82 µm	37 678
Monodisperse 100 µm	35 358
Monodisperse 150 µm	38 725

Table 4: Total droplet number in the computational domain.

process show similar total droplet numbers which are about 12 times larger than for simulation without secondary atomization. Differences observed between computations considering secondary atomization process are only due to the number of breakup steps undergone by the droplets. Indeed, biggest droplets (initial 150 µm droplets) are subject to more breakup steps than smallest ones (initial 50 µm droplets). The influence of initial distribution on the final droplet number is insignificant compared to the effects of atomization process which increases by a factor about 12 the total droplet number.

Figures 4 and 5 present axial and radial evolutions of droplet arithmetic mean diameter D_{10} for all computations realized. The irregular shape of curves concerning computations without secondary atomization is due to the limited droplet number

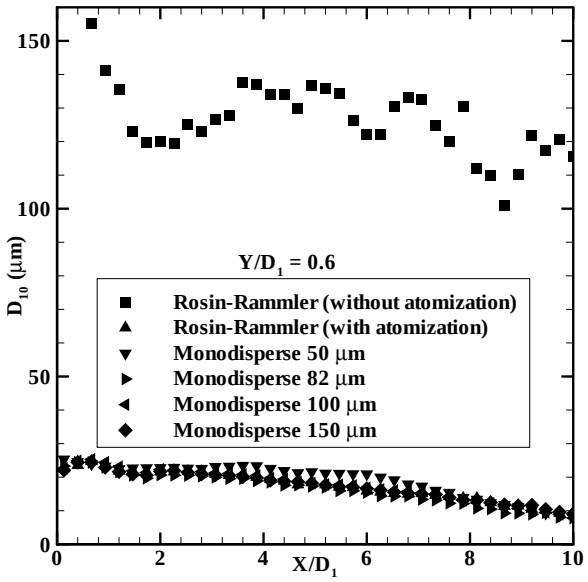

Figure 4: Axial evolution of droplet arithmetic mean diameter at radial location $Y/D_1 = 0.6$.

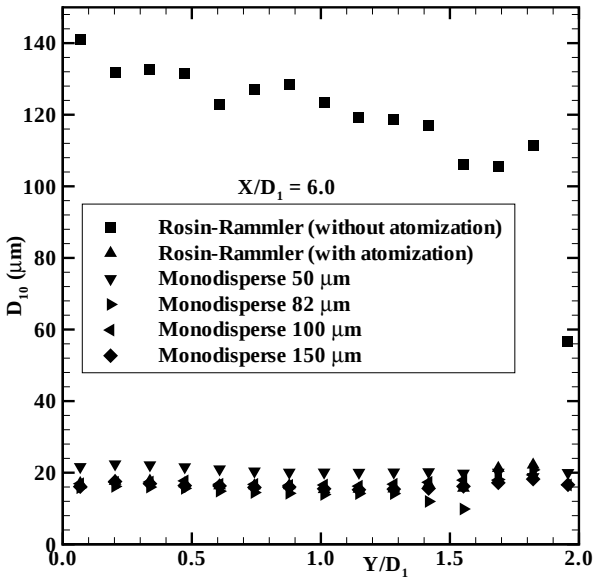

Figure 5: Radial evolution of droplet arithmetic mean diameter at axial location $X/D_1 = 6.0$.

used to realize the statistics on arithmetic mean diameter (see table 4). As in the case of total droplet number, the droplet arithmetic mean diameter is widely influenced by the atomization process. Indeed, this mean diameter is decreased by a factor of about 4-5 by the breakup phenomenon. The axial decreasing of this mean diameter (Fig. 4) in the case of the computation without secondary atomization is only due to the vaporization process (all computations are conducted using a classic D^2 law for vaporization), whereas in the cases using secondary atomization, the decreasing is due to a combination of breakup and vaporization phenomena. Radial evolutions of arithmetic mean diameter (Fig. 5) show quasi-constant values because of mainly axial droplet injection. Indeed, the maximal injection angle between droplet velocity and system axis obtained for $x = 0$ is about $20.5\,^\circ$. As in the case of axial evolutions, all computations considering secondary atomization process show a limited influence of initial distributions on droplet arithmetic mean diameter which is quasi-constant and equal to about $20\,\mu$m for all radial locations.

Figures 6 and 7 present axial and radial evolutions of Sauter mean diameter D_{32} for all computations carried out. As in the case of arithmetic mean diameter (Figs. 4 and 5), the influence of initial droplet distribution on Sauter mean diameter is insignificant. All computations with secondary atomization show similar values and similar shapes. The effect of secondary breakup process is pointed out by a comparison between computations using initial Rosin-Rammler distribution with and without fragmentation. The Sauter mean diameter is then decreased by a factor 4-5 when secondary atomization model is activated.

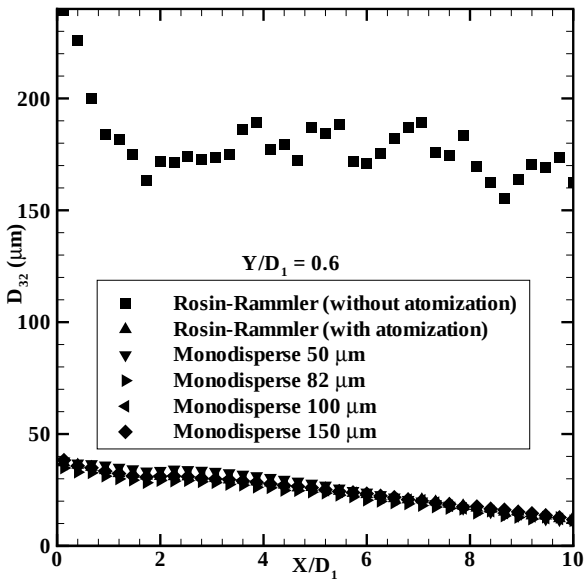

Figure 6: Axial evolution of droplet Sauter mean diameter at radial location $Y/D_1 = 0.6$.

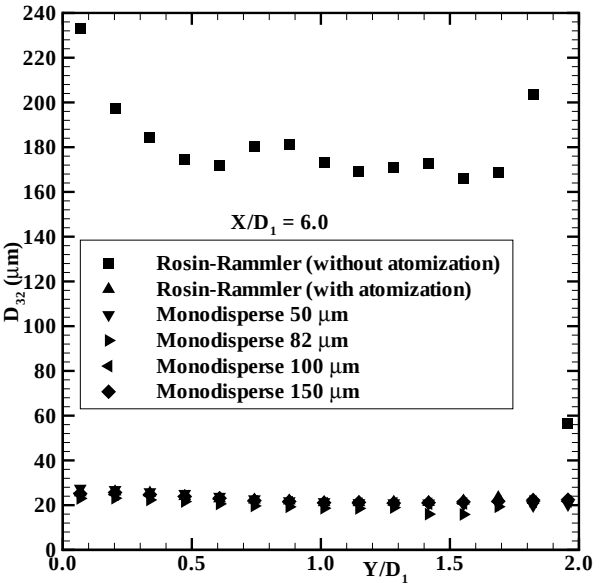

Figure 7: Radial evolution of droplet Sauter mean diameter at axial location $X/D_1 = 6.0$.

Table 5 presents parameters of a Rosin-Rammler distribution (see Eq. 5) determined for droplets existing in the computational domain for the different calculations. These parameters have been determined in a region far from the injection zone to eliminate the influence of atomization process. First of all, it is important to point out that these parameters have been determined with a confidence parameter R^2 larger than $98\,\%$, showing the good estimation for distributions. For the calculation without secondary atomization, these parameters are close to those of the initial droplet distribution introduced in the computational domain. Differences are only due to the vaporization process which decreases only slightly droplet sizes.

Initial distribution	N	D_{RR} (µm)	R^2
Rosin-Rammler (without atomization)	1.95	118.4	99.4 %
Rosin-Rammler (with atomization)	1.82	22.1	98.3 %
Monodisperse 50 µm	2.06	22.2	98.5 %
Monodisperse 82 µm	1.86	18.9	98.5 %
Monodisperse 100 µm	1.93	21.8	98.9 %
Monodisperse 150 µm	1.82	22.1	98.3 %

Table 5: Parameters of a Rosin-Rammler distribution far from the injection zone ($X/D_1 = 8.0$).

All other calculations with secondary atomization show very similar final distributions far from the injection zone, showing one more time the limited influence of initial droplet distribution on final spray structure. Differences observed between calculations using secondary atomization are only due to variations in droplet spatial distributions in the computational domain.

Flow properties

Figures 8, 9, 10 and 11 present axial and radial evolutions of hydrogen and oxygen mass fractions for all initial distributions considered. Because of mass conservation ($Y_{O_2} + Y_{H_2} = 1$) figures 8, 10 on one hand, and 9, 11 on other hand, show

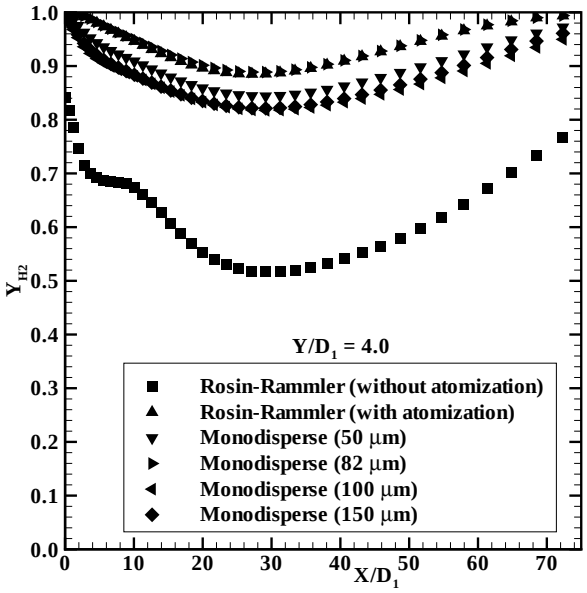

Figure 8: Axial evolution of H_2 mass fraction at radial location $Y/D_1 = 4.0$.

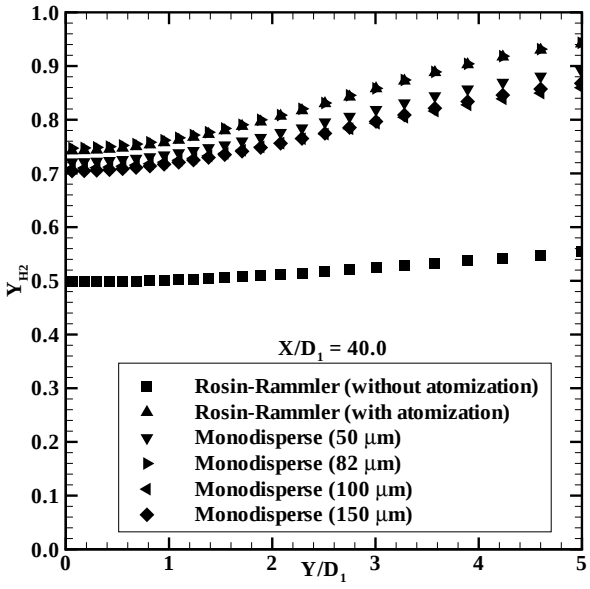

Figure 9: Radial evolution of H_2 mass fraction at axial location $X/D_1 = 40.0$.

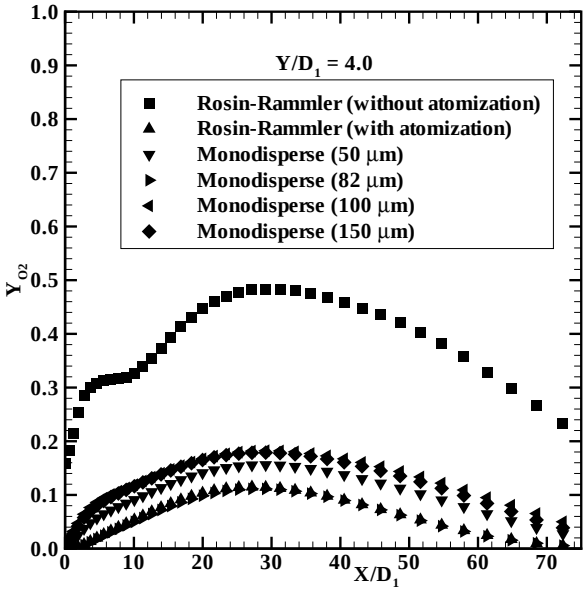

Figure 10: Axial evolution of O_2 mass fraction at radial location $Y/D_1 = 4.0$.

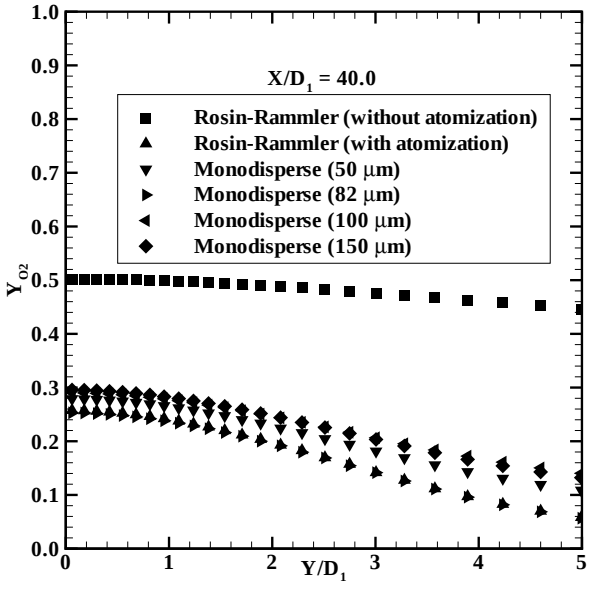

Figure 11: Radial evolution of O_2 mass fraction at axial location $X/D_1 = 40.0$.

complementary shapes. For computations with secondary atomization, the vapor generated is located near the system axis, limiting O_2 mass fraction values near the wall (at $Y/D_1 = 4.0$ on figures 10 and 11). Higher values observed for the computation without secondary atomization are due to the larger droplet lifetime because of their larger dimensions (see figures 4 and 5), permitting their vaporization far from the system axis. Finally, in the case of computation with secondary atomization, the oxygen vapor is confined near the system axis by the high velocity hydrogen jet. As for the spray properties, in the case of computations using secondary atomization, effects of initial distribution on final flow properties are very limited.

CONCLUSIONS

A secondary droplet breakup model has been developed from a previous experimental study conducted at LCSR. This model has been implemented in the SNECMA's THESEE code and used with the ONERA's MASCOTTE configuration. The influences of secondary atomization and initial distribution on final spray structure and final flow properties have been studied numerically. First, the secondary atomization phenomenon permits to observe an increasing droplet total number, associated with a decreasing of mean diameters (D_{10} and D_{32}). Second, the influence of initial droplet distribution on final spray structure in the cases of computations using secondary breakup is very limited. For the flow properties (O_2 and H_2 mass fractions) the O_2 vapor produced by the vaporization process is confined near the system axis by the high velocity hydrogen jet whereas, in the case of calculation without breakup, vapor is also generated near the system wall.

NOMENCLATURE

C	Breakup criterion	U_l	Liquid velocity, m/s
D	Droplet diameter, m	We	Weber number
D_{10}	Arithmetic mean diameter, m	x	Injection location on potential core, m
D_1, D_2, D_3	Coaxial injector dimensions, m	X	Distance in the axial direction, m
D_{32}	Sauter mean diameter, m	Y	Distance in the radial direction, m
D_{ini}	Initial droplet diameter, m		
D_{RR}	Parameter of the Rosin-Rammler distribution, m		**Greek symbols**
J	Momentum ratio		
L_C	Length of liquid potential core, m	α	Potential core angle
N	Parameter of the Rosin-Rammler distribution	θ	Injection angle
R^2	Confidence parameter	μ_g	Gas viscosity, kg/m/s
Re	Reynolds number	μ_l	Liquid viscosity, kg/m/s
T_{ini}	Droplet initiation time, s	$\nu_c(D)$	Cumulative probability
T_{BU}	Droplet total breakup time, s	ρ_g	Gas density, kg/m^3
U_0	Initial droplet velocity, m/s	ρ_l	Liquid density, kg/m^3
U_g	Gas velocity, m/s	σ	Surface tension, N/m

ACKNOWLEDGEMENTS

This work was supported by the joint CNRS/CNES/SNECMA/ONERA program "Combustion in Rocket Engines". Computations were performed with the support of CRIHAN. Emmabuel Bodèle was supported by a joint grant from ONERA and Conseil Régional de la Région Centre.

REFERENCES

1. M. Pilch and C.A. Erdman, Use of breakup time data and velocity history data to predict the maximum size of stable fragments for acceleration-induced breakup of a liquid drop, *International Journal of Multiphase Flow*, vol. 13, pp. 741–757, 1987.
2. R.S. Brodkey, *The phenomena of fluid motion*, Addison-Wesley, Reading, Mass, 1969.
3. A.A. Shraiber, A.M. Podvysotsky and V.V. Dubrovsky, Deformation and breakup of drops by aerodynamic forces, *Atomization and Sprays*, vol. 6, pp. 667–692, 1996.
4. G.I. Taylor, *The scientific papers of Sir G.I. Taylor*,Cambridge University Press, vol. 3, p. 457, 1963.
5. B.E. Gelfand, Droplet breakup phenomena in flows with velocity lag, *Progress in Energy and Combustion Science*, vol. 22, pp. 201–265, 1996.
6. E. Bodèle, Modélisation et simulation de l'atomisation secondaire et de la vaporisation turbulente. Application à la combustion cryotechnique., PhD Thesis, Orléans University, 2004.
7. B. Vieille, Étude exprimentale de l'atomisation de gouttes d'oxygène liquide. Influence de la pression., PhD thesis, Orléans University, 1998.
8. B. Vieille, C. Chauveau and I. Gökalp, Experimental studies on the breakup regimes of LOX droplets in helium, *16th ILASS Conference*, 1999.
9. A.A. Ranger and J.A. Nicholls, Aerodynamic shattering of liquid drops, *AIAA Journal*, vol. 7, pp. 285–290, 1969.
10. L. Vingert, M. Habiballah et P. Hervat, Mascotte : un banc de recherche pour la combustion cryotechnique, *Actes du colloques de Synthèse du groupe de recherche " Combustion dans les Moteurs Fusées "*, Cépaduès Éditions, pp. 178–201, 2001.
11. O.H. Haidn, Proceedings of the 2nd International Workshop on Rocket Combustion Modeling, Lampoldshausen, 2001.
12. E. Villermaux, Mixing and spray formation in coaxial jets, *Journal of Propulsion and Power*, vol. 14(5), pp. 807–817, 1998.
13. I. Care, Étude d'un injecteur coaxial assisté, PhD Thesis, Rouen University, 1990.